FERMILAB-PUB-18-302-TD
(accepted)
DOI: 10.1109/TASC.2018.2830703

Progress on HL-LHC Nb_3Sn magnets

E. Todesco, M. Annarella, G. Ambrosio, G. Apollinari, A. Ballarino, H. Bajas, M. Bajko, B. Bordini, R. Bossert, L. Bottura, E. Cavanna, D. Cheng, G. Chlachidze, G. De Rijk, J. DiMarco, P. Ferracin, J. Fleiter, M. Guinchard, A. Hafalia, E. Holik, S. Izquierdo Bermudez, F. Lackner, M. Marchevsky, C. Loeffler, A. Nobrega, J. C. Perez, S. Prestemon, E. Ravaioli, L. Rossi, G. L. Sabbi, T. Salmi, F. Savary, J. Schmalzle, S. Stoynev, T. Strauss, M. Tartaglia, G. Vallone, G. Velev, P. Wanderer, X. Wang, G. Willering, M. Yu

***Abstract*—The HL-LHC project aims at allowing to increase the collisions in the Large Hadron Collider by a factor ten in the decade 2025-2035. One essential element are the superconducting magnets around the interaction region points, where large aperture magnets will be installed to allow to further reduce the beam size in the interaction point. The core of this upgrade is the Nb_3Sn triplet, made of 150 mm aperture quadrupoles of in the range of 7-8 m. The project is being shared between CERN and US Accelerator Upgrade Program, based on the same design, and on two strand technologies. The project is ending the short model phase, and entering the prototype construction. We will report on the main results of the short model program, including quench performance and field quality. A second important element is the 11 T dipole that replacing a standard dipole makes space for additional collimators. The magnet is also ending the model development and entering the prototype phase. A critical point in the design of this magnet is the large current density, allowing increasing the field from 8 to 11 T with the same coil cross-section as in the LHC dipoles. This is also the first two-in-one Nb_3Sn magnet developed so far. We will report the main results on the test and the critical aspects.**

***Index Terms*—Superconducting magnets, Niobium-tin, Type II superconductors, superconducting coils.**

I. Introduction

After a first run in 2010-12 at 3.5-4 TeV per beam, corresponding to about half nominal energy, the Large Hadron Collider was operated at 6.5 TeV energy during the second run since 2015, with peak luminosity exceeding by 70% the nominal values [1]. LHC is supposed to reach an integrated luminosity of 300 fb^{-1} by 2025; this corresponds to about 2.5×10^{16} proton-proton collisions. In 2014, the High Luminosity LHC (HL-LHC) project was approved [2], with the aim of gathering ten times more luminosity in the decade 2025-2035. The project is based on new superconducting magnets [3], and is complemented by an upgrade of the LHC injectors [4], foreseen for 2019-20. The HL-LHC project relies on (i) an increase of beam intensity by a factor 2, requiring the installation of additional collimators, (ii) the reduction of the beam size in the interaction region by a factor 2, requiring large aperture magnets around ATLAS and CMS and (iii) the use of crab cavities to compensate luminosity loss due to the crossing angle. These steps are complemented by (i) an upgrade of the cryogenic plants, (ii) new civil engineering - both underground and surface - to accommodate new equipment and (iii) a superconducting link relying on MgB_2 [5] to bring ~100 kA in the LHC tunnel to power the new magnets.

The project relies on two different types of Nb_3Sn magnets operating in the range of 12 T peak field. The higher intensity may require additional collimators to reduce beam losses in the magnets. Few of them need to be installed in zones covered by LHC dipoles: for this reason the development of a Nb_3Sn 11 T dipole was launched in 2010 [6]. The program aimed at replacing a 14.3-m-long dipole with a 11-m-long Nb_3Sn magnet and a room temperature collimator and was complemented by a US program at FNAL [8]. Ten units were initially foreseen; successive studies, complemented by data from LHC operation, reduced the need to two units to be installed in 2019-20 [9].

The rate of collisions is increased via (i) more intense beams and (i) high probability of collision induced by the reduction of the size of the beam in the interaction points. To reach this aim, one needs larger aperture magnets around ATLAS and CMS, namely the triplet, the separation and the recombination dipole, and the associated correctors. In 2001 [10] it was proposed to increase the present 70 mm aperture of the triplet to 90 mm to allow doubling the collision rate. In 2004 the LHC Accelerator Research Program (LARP [11]) was approved to develop Nb_3Sn large aperture quadrupoles for the LHC luminosity upgrade. A design study supported by UE funds was launched in 2011 [12], and in July 2012 a very ambitious choice of 150 mm aperture was done [13], aiming at a four-fold increase of the collision rate thanks to a half beam size in the interaction point. The aperture also includes a 16-mm-thick tungsten absorber to bring the heat load and the radiation damage on the magnets in the HL-LHC era back to the LHC values. This aperture choice required an increase of the cryostat diameter, bringing it at the limit of what can fit in the LHC tunnel. Four Nb_3Sn triplets will be installed in 2024-25, half of them built by the US HL-LHC Accelerator Upgrade Project. There is a total of twenty 4.2-m-long magnets made in US, plus ten 7.15-m-long magnets built at CERN and in the EU industry (including spares). CERN and US carry out since 2012 a joint program of R&D, heavily relying on LARP results [14].

Both programs are now in the transition from the short model phase to the first full-length prototypes. In this paper we will outline the present status and the main challenges of these

E. Todesco, A. Ballarino, H. Bajas, M. Bajko, B. Bordini, L. Bottura, E. Cavanna, G. De Rijk, P. Ferracin, J. Fleiter, M. Guinchard, S. Izquierdo Bermudez, F. Lackner, C. Loeffler, J. C. Perez, L. Rossi, F. Savary, G. Vallone, G. Willering, are with CERN, TE Department, Geneva 23 1211 Switzerland (e-mail: Ezio.todesco@cern.ch).

G. Ambrosio, G. Apollinari, R. Bossert, G. Chlachidze, J. DiMarco, E. Holik, A. Nobrega, J. Schmalzle, S. Stoynev, T. Strauss, M. Tartaglia, G. Velev, M. Yu, are with FNAL, D. Cheng, A. Hafalia, M. Marchevsky, S. Prestemon, E. Ravaioli, G. L. Sabbi, X. Wang, are with LBNL , M. Annarella, P. Wanderer, are with BNL, T. Salmi is with Tampere University.

This document was prepared by HL-LHC collaboration using the resources of the Fermi National Accelerator Laboratory (Fermilab), a U.S. Department of Energy, Office of Science, HEP User Facility. Fermilab is managed by Fermi Research Alliance, LLC (FRA), acting under Contract No. DE-AC02-07CH11359.

magnets, which represent a 4 T leap forward in the magnet technology for particle accelerators. At the same time, we will compare the design parameters with the first baseline that is being produced for a 16 T magnet [15] in the framework of the Future Circular Collider [16] – a 50 TeV per beam accelerator with a 100 km circumference.

II. The 12 T Challenge

A. Current density, coil width, margin

In a dipole based on sector coil of angle φ the field is proportional to the current density *j* and to the coil width *w*

$$B = \frac{2\mu_0}{\pi} jw \sin\varphi \quad (1)$$

For a quadrupole of aperture radius *r* and coil width *w* the gradient is proportional to

$$G = \frac{\mu_0}{\pi} j \log\left(1 + \frac{w}{r}\right) \sin 2\varphi \quad (2)$$

A higher field/gradient can be obtained by increasing the coil width and/or the current density. The first path is the less difficult, the main drawbacks being (i) the larger quantity of conductor, (ii) a less compact magnet and (iii) a more complex coil fabrication, having to deal with larger transverse sizes. The second path is more difficult since it hits several physical limits: (i) the protection constraints for long magnets, where the energy has to be absorbed by the coil enthalpy, (ii) the strain on the conductor induced by electromagnetic forces, (iii) instabilities related to the self-field and to the magnetization. Magnets in previous particle accelerators [17-20] operated with a current density in the strand (the so-called engineering current density j_{eng}) between 500 and 600 A/mm^2, and coil width in the range of 10 to 30 mm (see Fig. 1). High field Nb_3Sn models developed in LBNL were successfully built with a coil width of 45 mm [21,22], and reached maximum peak fields of ~13.5 T. Recently, a giant leap has been made with FrescaII, a 1.5-m-long large-aperture dipole with a coil width of 80 mm; the magnet reached 13 T at 70% of the loadline and 350 A/mm^2 strand current density [23]. Present targets for the 16 T dipole [15] required for the Future Circular Collider study (cos theta design) are a coil width of 50 mm and a graded coil with current densities of 500 A/mm^2 and 800 A/mm^2 [24].

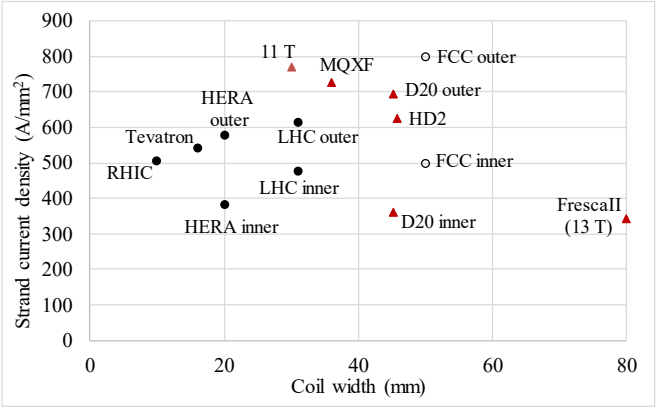

Fig. 1: Coil width and strand current density for accelerator magnets. For D20 and HD2 data relative to max field reached are given. Dots for Nb-Ti, triangles for Nb3Sn and empty circles for FCC targets.

TABLE I
Main Parameters of the 11 T dipole and MQXF, Compared to LHC dipole and FFC dipole (cosθ) proposal

		MQXF	11 T	LHC dipole	FCC cosθ
Aperture	(mm)	150	60	56	50
Lenght	(m)	7.15	5.3	14.3	14.3
Field	(T)		11.2	8.3	16
Gradient	(T/m)	132.6			
Peak field	(T)	11.4	11.6	8.7	16.5
Current	(kA)	16.47	11.85	11.85	11.23
Short sample current	(kA)	21.12	14.81	13.78	
Loadline fraction	(%)	78%	80%	86%	86%
Strand diameter	(mm)	0.85	0.7	1.065/0.825	1.1/07
N. Strands	(adim)	40	40	28/36	22/36
Cu/No_Cu	(adim)	1.2	1.15	1.65/1.95	0.9/2.2
Keystone angle	(degrees)	0.50	0.70	1.25/0.90	0.5/0.6
Strand current density	(A/mm^2)	726	770	475/616	540/790
Coil width	(mm)	36	30	31	50
Stored energy	(MJ)	8.37	5.313	7.0	37
Strand energy density	(J/mm^3)	0.129	0.145	0.072	0.200
Pressure due to e.m. forces	(Mpa)	101	97	44/57	92/136

B. Length

The management of thermal contractions and dilatations (from 1.9 K during magnet operation to 650º C during coil reaction) of the different magnet components is one of the main challenges of the Nb_3Sn technology; they scale with the magnet length. One-meter-long models were built since the 90's [25,26]. In 2008, LARP successfully proved the technology up to 3.4-m-long coils [27]. The extension was not trivial, requiring a segmentation of the Al shells to minimize the accumulation of longitudinal stresses. HL-LHC magnets will bring this range to 5-7 m; the final target for FCC is 15 m long dipoles as in the LHC. The 11 T dipole magnet, initially foreseen as one 11-m-long magnet, has been split in two units of 5.3 m. The MQXF program consists of a 7.15-m-long Q2 built at CERN, whereas the US program went for a split Q1/Q3 magnet made of two 4.2-m-long units to mitigate the risks related to long coils. The two magnets can be placed in the same cold mass at a minimal distance of ~500 mm, so the loss in terms of integrated gradient is of the order of 5%. The magnet split entails a 20% higher cost for the manufacturing, and the need of two production lines for the coils.

C. Margin and current density

The specification for the critical current in the superconductor is 2280-2450 A/mm^2 at 12 T, 4.2 K and 1280 A/mm^2 at 15 T, 4.2 K [13]. Two strategies were used: the 11 T dipole project set the specification at 12 T, i.e. around the operational peak field; the MQXF project set the specification at 15 T, i.e. around the short sample value.

For the MQXF, the initial value of 1400 A/mm^2 at 15 T has been reduced by 10% in 2014 to include the whole production. Data show that this specification is well kept in the series production (see Fig. 2). Similar values for the production carried out in the US are given in [28]. For the 11 T dipole a fraction of the production is below the specification of 2450

A/mm^2 at 12 T (see Fig. 3).

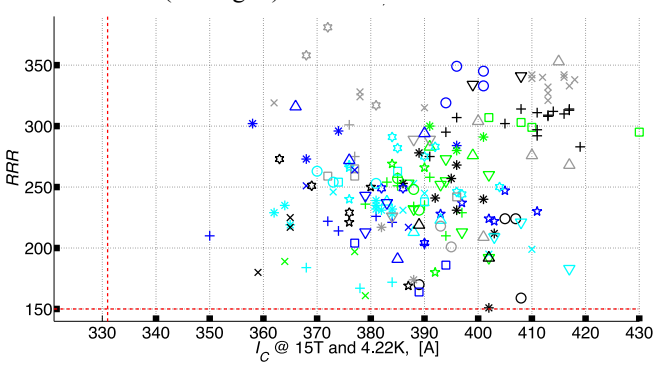

Fig. 2: Critical current at 15 T and RRR for 0.85 mm strand; different symbols correspond to different batches.

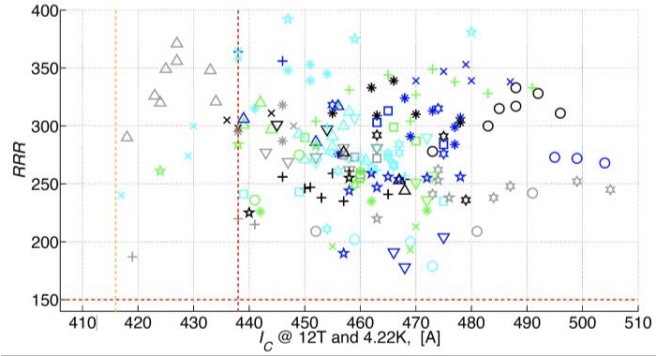

Fig. 3: Critical current at 12 T and RRR for 0.7 mm strand; different symbols correspond to different batches.

Both magnets are designed to operate at approximately 80% of the short sample (see Fig. 4, where magnet loadlines and working point are shown for 11 T dipole, MQXF, and also for LHC main dipoles and baseline of a future FCC dipole – note that the plot is given for the superconductor current density to avoid having different critical surfaces for different Cu/no_Cu ratios). For the MQXF, the 10% reduction of the current specification implied a loss of 3% on the short sample current (see Fig. 5). To recover an adequate margin in 2014 the magnet current has been reduced by 5%, bringing the operational current to 78% of the short sample. This was compensated by the increase of the magnet length by 5%.

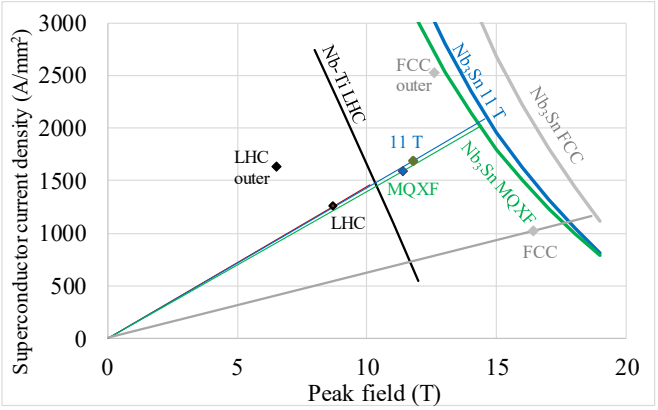

Fig. 4: Critical surface and loadlines at 1.9 K for LHC dipoles (inner layer), MQXF and 11 T dipole, and present proposal for FCC dipoles.

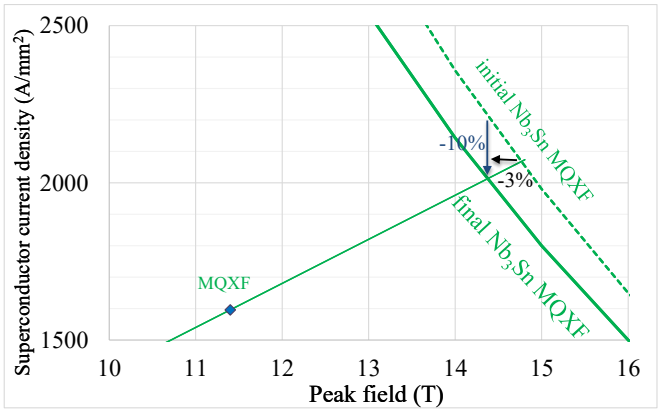

Fig. 5: Reduction of 10% in critical current of the strand, giving a reduction of 3% of short sample current in MQXF

D. Strand

The MQXF cable is made both with RRP strand 108/127 (all US magnets, plus eight CERN magnets), and with PIT 192 strand (two CERN magnets); the 11 T dipole cable is made with the RRP 108/127, see Table II. During the short model phase, RRP wire with finer filaments has also been explored. The PIT strand layout went through an iteration of the layout (insertion of a bundle barrier) to improve the current density and the RRR [29]. The RRP 108/127, which has been the workhorse of LARP together with the RRP 54/61, has been selected for a sufficiently thin filament for both applications and for the lower cost. The copper / non copper fraction of 1.2/1.15 is at the limit of the protection requirements (see Section II.I).

Flux jumps require a variable threshold for protection, with 300 mV at low field and 100 mV at high field. This has been made possible through a new hardware development.

TABLE II
STRAND FOR MQXF AND 11 T DIPOLE (IN BOLD THE CHOICE FOR THE SERIES, PIT NOT SHOWN FOR 11 T DIPOLE)

MQXF					11 T			
PIT	PIT	**RRP**	RRP	Technology	**RRP**	RRP	RRP	RRP
192 bundle	192	**108/127**	132/169	Layout	**108/127**	132/169	144/169	150/169
1.15	1.22	**1.19**	1.22	Cu/ NoCu	**1.19**	1.28	1.08	1
39	41	**55**	50	Subelement size (μm)	**46**	41	41	41
Circ	Circ	**Circ**	Hex	Subelement shape	**Hex**	Hex	Hex	Hex
	4	3	5	Short coils tested	2	4		3

E. Cable

Both magnets make use of 40 strand cable with moderate keystone angle. The large aspect ratio of this cable required a careful optimization of the cable parameters [30]; final choice was a trade-off between a good compaction (needed to avoid strand pop out during winding) and a low deformation of the strands (to avoid the degradation of the critical current). Both 11 T dipole and MQXF makes use of a special tool to avoid strand pop up when winding coil ends, developed in LBNL. The MQXF cable dimensions were iterated at the beginning of the short model phase, reducing the keystone angle from 0.55 to 0.4 to reduce the critical current degradation.

A total of 10 km were produced for the MQXF and 14 km for the 11 T dipole (short models and prototypes). For the prototypes, 13 and 9 unit lengths were produced. One MQXF

cable for prototype had a cross-over, and the length was reused for short models. Recent studies show that the degradation of critical current due to cross-over is tolerable (i.e. a few percent [31]), but the issues of instabilities induced by current redistribution are still open.

F. Insulation

Cable insulation is given by a 66-tex braided S2 fiberglass. The 11 T dipole uses an additional a 50-μm-thick C shaped mica sheet. The insulation thickness after reaction is 0.145 mm for MQXF and 0.100 mm for the 11 T dipole.

Recent tests with Fuji paper showed an accumulation of stress at the edge of the cable, where the mica sheet is present on both sides. In the hypothesis of an accumulation of the gaps in a single block, this can induce a variation of coil thickness of 0.5 mm, i.e. pre-stress variations of the order of 150 MPa (see next section). An iteration to reduce the gap is ongoing.

G. Coil manufacturing and coil size

The coil manufacturing follows similar procedures in 11 T dipole and MQXF. Winding begins from the layer jump with the inner layer, and the outer layer is wound on the inner after curing. Reaction follows the same cycles, with a plateau of 50 h at 650º C. A relevant difference is the impregnation: in the 11 T dipole the pole is not impregnated with the coil, leaving the possibility of an additional degree of freedom for shimming and allowing the detachment of the coil from the pole during powering. This technology follows the one developed for the CERN-Elin dipole [25]. The MQXF has a pole impregnated with the coil, following the LARP design [11]. At the moment of writing, 24 MQXF (16 at CERN and 8 at US) and eighteen 11 T dipole short coils have been manufactured, including practice and low-grade coils; among them, twelve MQXF and nine 11 T dipole coils have been tested in short models (see Section II.J).

A critical parameter is the control of the coil dimensions: the arc length of the coil shall be within 0.1% from nominal dimensions to allow reaching the nominal pre-stress and the nominal geometry (i.e. field quality) with nominal shimming. A 0.1% change in coil dimension implies a change of 15 MPa in the coil compression at 1.9 K, which is at the limit of the required control in pre-stress. Since both 11 T dipole and MQXF have accidentally the same coil arc length of 100 mm, a 0.1% change in the coil arc length translates in the same tolerance of 0.05 mm at the pole.

From the point of view of field quality, a change of 0.05 mm at the pole gives a change of b_3 of ~2.5 units in a dipole and a change of b_6 of ~1 units for a quadrupole; in both cases these changes are at the limit of the field quality requirements.

Both in MQXF and 11 T dipole, non-nominal shims are being applied when coil size difference from nominal is larger than 0.05 mm, with a probably excessive granularity of 0.025 mm. The shimming is uniform along the magnet axis, even though the variations along the axis can reach ±0.1 mm, as shown in Fig. 6 [32]. The same figure also shows a variation of coil size average of the order of 0.4 mm. Similar initial variations were also experienced in the initial part of the LHC production, and reaching the 0.1 mm control in the coil size is the main challenge of both projects.

An additional challenge of Nb_3Sn is that the coil elastic modulus is about twice of Nb-Ti coils. Therefore the same relative variation of coil size gives a double effect on prestress in Nb_3Sn coils with respect to Nb-Ti.

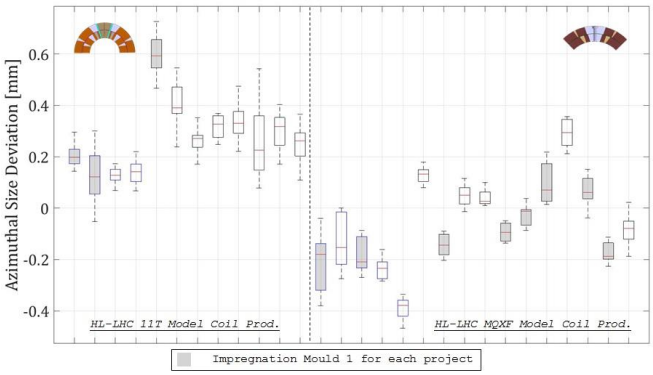

Fig. 6: Measured arc coil lengths for 12 coils of the 11 T dipole and for 16 coils of MQXF. Horizontal axis is the coil progressive number. The candlestick represents the upper and lower quartile (box) and the total spread (error bar)

H. Structure and prestress

A simple way of comparing forces in magnet design, independently of the mechanical structure, is the sum of the azimuthal components of the forces in the coil, divided by the coil width. This gives an indication of the compression in the midplane induced by the electromagnetic forces, ignoring friction, structure deformation, prestress etc. In the LHC dipoles, the accumulation of the electromagnetic forces compresses the coil in the midplane with 70 MPa, see Table I. This value is increased by 50% to ~100 MPa for the 11 T dipole and for the MQXF (see Table I). To avoid the detachment of the coil from the pole, coils are pre-stressed during assembly so that the coil is still compressed by the pole at nominal current using a well-known strategy that dates back to the 70's [33]. This goal is reached through two different structures (see Figs. 7 and 8). The 11 T dipole imposes a fixed dimension through collaring, with main load applied at room temperature. The MQXF imposes a stress through bladder and keys, and most of the load is applied during the cool down through the thermal contraction of the Al shell.

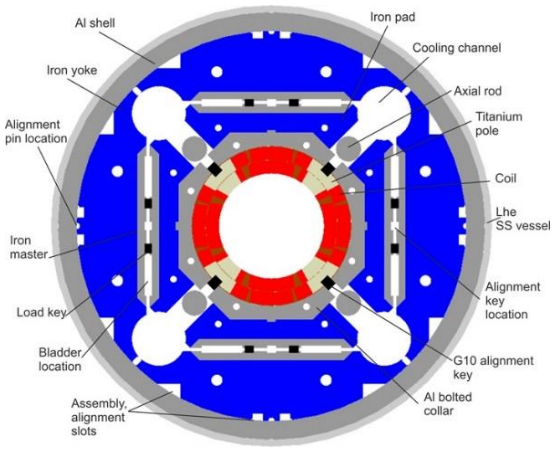

Fig. 7: MQXF cross-section

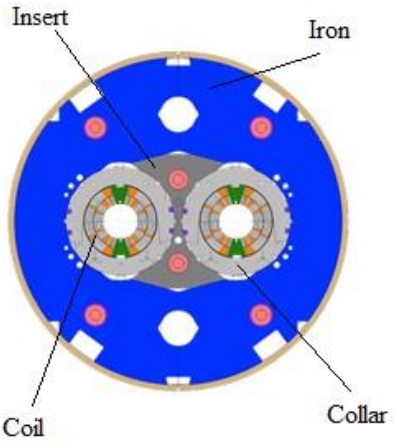

Fig. 8: 11 T dipole cross-section

In Nb_3Sn impregnated coils degradation of critical current starts at 150-200 MPa [34] – this narrows the window of required preloads. Accounting for tolerances of coil size described in the previous section, and tolerances in the structure components, centering the full preload without hitting cable degradation would look like a mission impossible. Indeed, two aspects have to be pointed out: first, even a 15% degradation in critical current reduces the short sample current of about 5% (see Fig. 5), and therefore can still be invisible for a magnet working at 80-85% of short sample. Second, the strain gauges show in both cases that the magnet can still train when the pole is unloaded (see Fig. 9 for MQXF and Fig. 10 for the 11 T dipole). The experience of MQXF short models, loaded with pre-stress ranging from 90 to 130 MPa, show that the window of possible loading to reach nominal performance is wide.

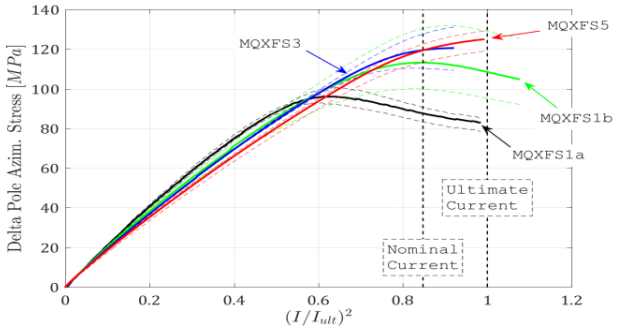

Fig. 9: MQXF unloading during powering: measured pole azimuthal stress versus square of the current.

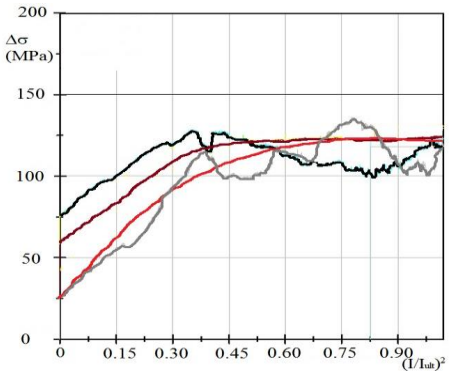

Fig. 10: 11 T dipole unloading during powering: measured pole azimuthal stress versus square of the current in the second and third short model of the 11 T dipole (different curves corresponds to different coils)

Strain gauges are very important to have a control of the load in operational conditions. In MQXF strain gauges are glued on the coil pole, parallel to the beam direction. In the 11 T dipole this position cannot be used due to the pole indent to release stress and therefore they have to be placed in the collar nose laminations, perpendicular to the beam direction. In both cases (see Fig. 9 and 10) one obtains reliable data for the pole unloading, even though the 11 T dipole position requires FEM to reconstruct the stress in the coil pole.

I. Protection

The protection strategy for both magnets cannot rely on energy extraction, and the energy has to be dumped in the coil. With respect to the LHC dipoles there is a non-negligible increase of the ratio between stored energy and the strand volume, that increases from 0.072 J/mm^3 to 0.129 J/mm^3 (MQXF) and 0.145 J/mm^3 (11 T dipole), see Table I. The maximum hotspot temperature is set at 350 K, and this gives a protection time margin (time allowed to detect the quench and to bring all the coil to resistive state [35]) of 45 ms for MQXF and 38 ms for the 11 T dipole.

Protection in the 11 T dipole is done through quench heaters on the outer layer, impregnated with the coil following the LARP design. For the MQXF, even though protection is less challenging, an additional safety system is added, and either inner layer quench heaters [36] or CLIQ [37] will be used. The reason of this redundancy are the installation features, a MQXF magnet being much more cumbersome to be replaced than an 11 T dipole, especially if located in Q1 position. Each one of these systems gives a reduction of the hotspot temperature of the order of 70 K. A selection between the two options will be carried out at the end of the prototype phase.

J. Performance

Three MQXF short models and five 11 T dipole single aperture short models, plus one double aperture, have been tested. The performances are shown in Figs. 11-18 and in Table III. Note that the HL-LHC project requires the ability to reach ultimate current, i.e. 8% more than nominal. The magnet label change (progressive letters a, b, c …) if a coil is replaced or if the prestress (axial or azimuthal) is increased.

TABLE III
QUENCH PEROFMANCE OF MQXF, 11 T SHORT MODELS AND COMPARISON TO LHC MAIN DIPOLES (ATC=AFTER THERMAL CYCLE)

	MQXF	11 T	LHC
First quench/short sample	69%±4%	57%±8%	83%±13%
Quench to nominal	6	10	0.6
Quench to ultimate	23	20	
% loss ATC	0.5%±0.8%	3%±3%	5%±8%
Quench to nominal ATC	0		0.3
Quench to ultimate ATC	0		1.5
Coils tested	12	10	4984

One can make the following remarks:

- Out of the 21 short coils tested, all reached at least 50% of

short sample without quench.

- The design proved the ability to reach nominal and ultimate current, but the reproducibility is not given. Nominal was attained for 3/3 in MQXF and 4/5 in 11 T dipole. Ultimate current has been reached for 2/3 of MQXF and for 2/5 of the 11 T dipoles.
- First quench: The first quench level is lower than Nb-Ti dipoles, i.e. training starts at 70% of short sample for MQXF and at 60% for 11 T dipole.
- Virgin training length: with respect to Nb-Ti one has a longer training, with 5-10 quenches to reach nominal.
- Memory after thermal cycle: For magnet operation the most relevant parameter is the number of quenches to nominal after thermal cycle: both 11 T dipole (1 double aperture and 2 single apertures magnets) and MQXF (3 magnets) show a very small loss of memory compared to Nb-Ti.
- Performance at 4.2 K: For MQXF performance at 4.2 K is not reduced with respect to the last quench at 1.9 K, reaching more than 90% of short sample limit. This excludes a critical current degradation larger than ~30%. Note that in the MQXF models no attempt has been made until now to train above the 18-18.5 kA, so we can give only an upper limit to possible degradation. For 11 T dipole no reduction is observed in three cases out of five: in the other two, a ~1 kA reduction is observed, i.e. the magnet reach 80-85% of short sample limit at 4.2 K. This is compatible with a degradation of critical current larger than 30%.
- Double aperture: The only case of assembly of double aperture with two coils already trained in single aperture configuration showed ability of reaching nominal without quench.
- Detraining and erratic behaviour: Some magnets experienced a non-negligible detraining.
- Quench location: Two 11 T dipole short models have mid-plane quenches, interpreted as excessive pressure leading to large conductor degradation. This is also compatible with the observation on the 4.2 K behavior. An iteration to reduce pre-stress is being carried out.

Concerning individual magnets one can give the following remarks:

- First short model MQXFS1 (RRP coils, two from CERN and two from US) reached ultimate, with perfect memory and same performance at 4.5 K (see Fig. 11). After a azimuthal prestress increase it reached 18.5 kA, i.e. 86% on the loadline.
- Second short model MQXFS3 (RRP coils, 3 from CERN and 1 from US) had a significant detraining in one coil (see Fig. 12). Performance was recovered after a ramp rate test; it reached nominal but not ultimate. After thermal cycle and a axial prestress increase, the magnet was still limited at 16.7 kA, few hundered ampere above nominal. Indeed, the magnet reached 17.7 kA at 1.9 K with 200 A/s ramp rate, and also at 4.2 K, with nominal ramp rate. Both events indicate the presence of nontrivial physics (not a simple degradation due to prestress) limiting the magnet, which can be bypassed by high ramp rate or higher operational temperature.
- The limiting coil has been replaced and the new assembly will be tested in fall 2017.
- Third short model MQXFS5 (PIT coils) reached smoothly ultimate and had perfect memory (see Fig. 13).

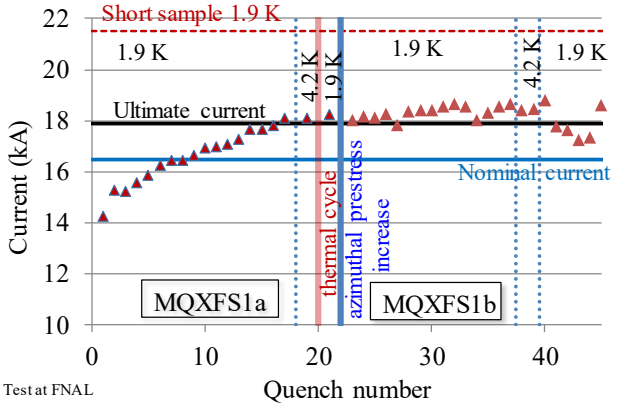

Fig. 11: Training of MQXFS1

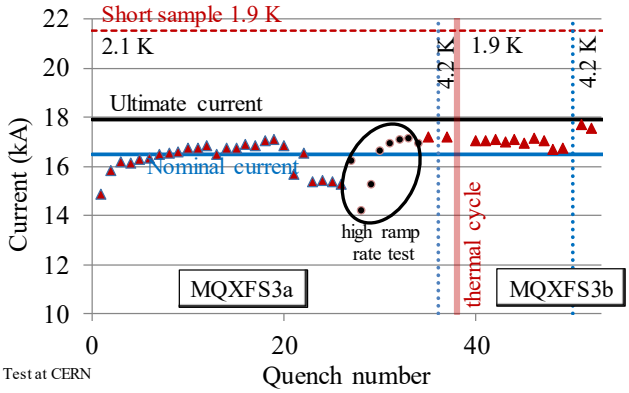

Fig. 12: Training of MQXFS3

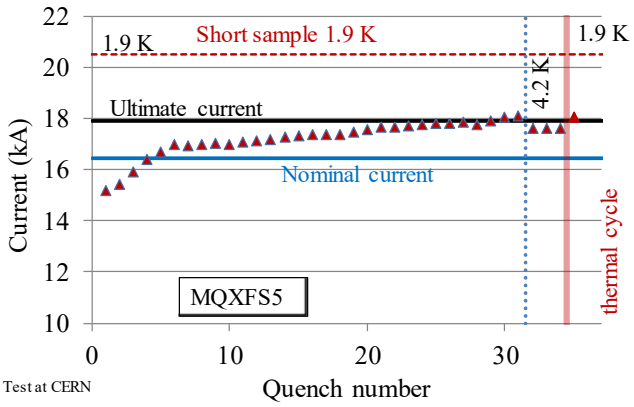

Fig. 13: Training of MQXFS5

- The first 11 T dipole short model (SP101) reached nominal, but showed detraining (see Fig. 14). After thermal cycle a loss of 800 A was observed: one coil was limiting magnet performance and was replaced and

assembled in 102.

- The second 11 T dipole short model (SP102) used one coil from 101 and a new coil (see Fig. 15). It reached ultimate but had some detraining and erratic behavior between ultimate and nominal. A good memory after thermal cycle has been observed. At 4.2 K there is a loss of 1 kA.
- The third 11 T dipole short model (SP103) reached ultimate without detraining (see Fig. 16). Also in this case, a loss of 1 kA at 4.2 K is observed. Thermal cycle has not been done, but the collared coil was used for the double aperture DP101.
- The fourth 11 T dipole short model (SP104) barely reached nominal (see Fig. 17) and had a limiting coil, which has been replaced after the test. The new collared coil will be placed in the second double aperture model DP102.
- The fifth 11 T dipole short model (SP105) reached nominal but not ultimate (see Fig. 18). This collared coil has been recollared with lower prestress and will be tested in the second double aperture model.
- The first double aperture magnet (DP101) was made with SP102 and SP103 apertures, and reached nominal without quench and ultimate very rapidly (see Fig. 19).

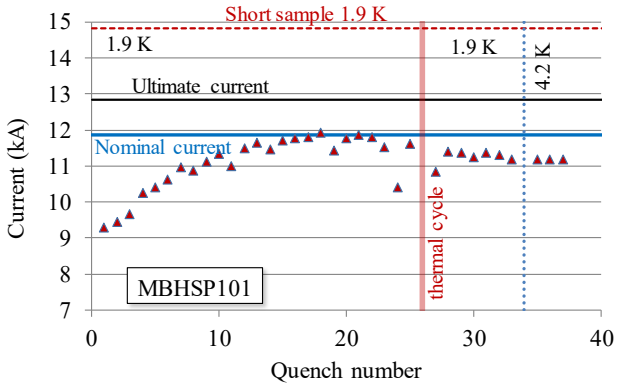

Fig. 14: Training of MBHSP101

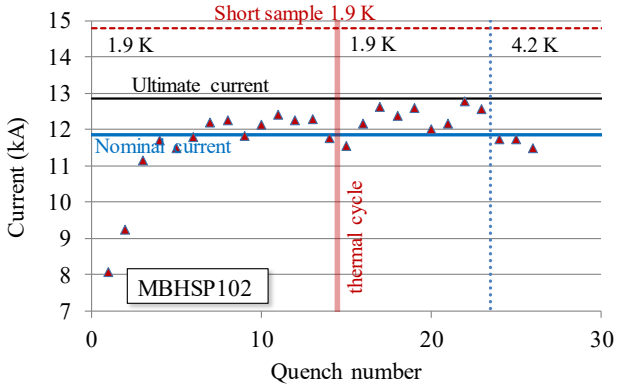

Fig. 15: Training of MBHSP102

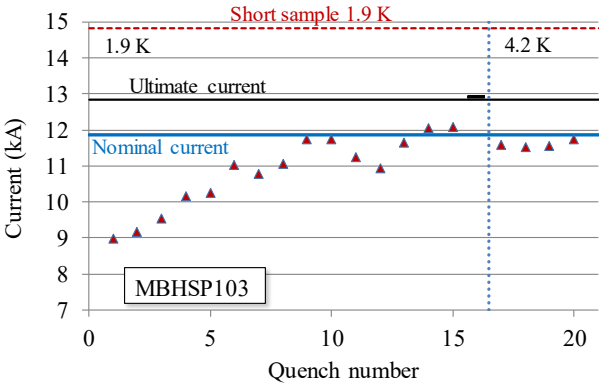

Fig. 16: Training of MBHSP103

The short model program will be complemented by (i) two additional models for MQXF, one with final RRP and one with final PIT conductor, to be tested in 2018 and (ii) one additional 11 T double aperture DP102, plus two single aperture with PIT conductor, and one single aperture with RRP final strand. As a technological development, not required for 11 T dipole project, an additional single aperture will have interlayer quench heaters..

Prototype construction is ongoing. The most advanced is the 4-m-long US MQXF, which is under test at the moment of writing, and had a first quench at 75% of short sample. The 11 T dipole prototype test is foreseen for beginning of 2018, and the test of the 7.15-m-long MQXF prototype for beginning of 2019.

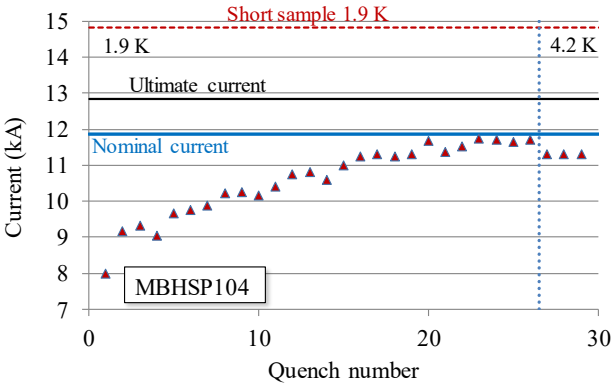

Fig. 17: Training of MBHSP104

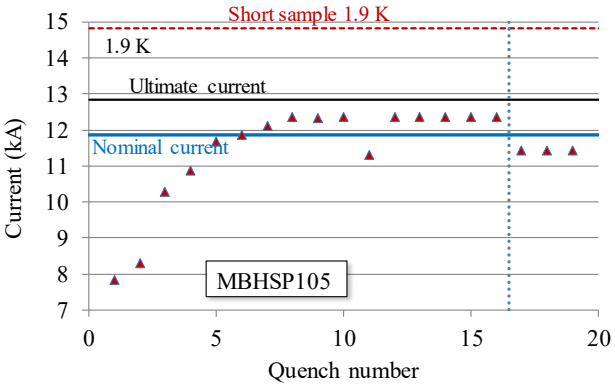

Fig. 18: Training of MBHSP105

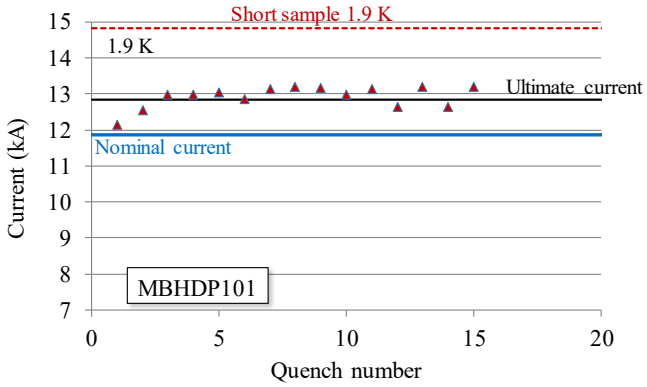

Fig. 19: Training of MBHSD101

III. Conclusion

The HL-LHC project will rely on two Nb_3Sn magnets operating at a 12 T peak field. These magnets are exploring an unprecedented strand current density of 700-800 A/mm^2. The main challenges, apart from the current density, are the management of the thermal contractions, the dimensional tolerances of the coil, and the control of pre-stress during the assembly. The short model program is approaching to the end, with 20 coils tested in the nominal configurations. The prototype phase has started, and several long coils have been already manufactured, with crucial tests expected in 2018.

References

[1] J. Wenninger, et al., "Approaching the nominal performance at the LHC", International Particle Accelerator Conference, 2017.

[2] G. Apollinari, ed. et al., "High-Luminosity Large Hadron Collider Technical Design Report", CERN Yellow Report 2017-007.

[3] L. Bottura, G. de Rijk, L. Rossi, E: Todesco, "Advanced accelerator magnets for upgrading the LHC", IEEE Trans. Appl. Supercond., Vol. 22 (2012) 4002008.

[4] H. Damerau, ed. et.al., "LHC injectors upgrade Technical Design Report Vol. I: Protons", CERN-ACC-2014-0337.

[5] A. Ballarino, "Development of superconducting links for the Large Hadron Collider machine", Supercond. Sci. Technol. Vol. 27 (2014) 044024.

[6] G. De Rijk, A. Milanese, E. Todesco, `11 Tesla Nb3Sn dipoles for phase II collimation in the Large Hadron Collider', CERN SLHC Project Note **19** (2010).

[7] M. Karppinen, et al., "Design of 11 T twin aperture Nb3Sn dipole Demonstrator Magnet for LHC upgrades", IEEE Trans. Appl. Supercond., Vol. 22 (2012) 4901504.

[8] A. Zlobin, et al., "Development and test of a single-aperture 11 T Nb_3Sn demonstrator dipole for LHC upgrades", IEEE Trans. Appl. Supercond., Vol. 23 (2013) 4000904.

[9] F. Savary *et al*., "The 11 T dipoles for HL-LHC: status and plan," IEEE Trans. Appl. Supercond., vol. 26, 2016, Art. ID. 4005305.

[10] T. Sen, et al., "Second Generation High Gradient Quadrupoles for the LHC Interaction Regions", proceedings of Particle Accelerator Conference 2001, 3421-3.

[11] S. Gourlay, et al., "Magnet R&D for the US LHC Accelerator Research Program (LARP)", IEEE Trans. Appl. Supercond., Vol. 16 (2006) 324-7.

[12] L. Rossi and O. Bruning, "High luminosity large hadron collider: A description for the european strategy preparatory group," CERN, Geneva, Switzerland, Rep. CERN -ATS- 2012-236, Nov. 1, 2011. [Online]. Available: http://hilumilhc.web.cern.ch/

[13] E. Todesco *et al*., "A first baseline for the magnets in the high luminosity LHC insertion regions," IEEE Trans. Appl. Supercond., vol. 24, no. 3, Jun. 2014, Art. ID. 4003305.

[14] P. Ferracin, et al., "Development of MQXF: the Nb_3Sn low-beta quadrupole for the Hilumi LHC," IEEE Trans. Appl. Supercond., vol. 26, 2016, Art. ID. 4000207.

[15] D. Tommasini, et al., "The 16 T dipole development program for FCC", IEEE Trans. Appl. Supercond., vol. 27, no. 4, Jun. 2017, Art. ID. 4000405.

[16] M. Benedikt, F. Zimmermann, "Status of the future circular collider study", RuPAC 2016 34-38, www.jacow.org

[17] R. Hanft, et al., "Magnetic field properties of Fermilab Energy Saver Dipoles", TM-1182, 1630, 03/1983

[18] S. Wolff, "The superconducting magnet system for HERA", proceedings of MT19, ed. By C. Marinucci and P. Waymuth (Zurich, SIN, 1995).

[19] M. Anerella et al., "The RHIC magnet system", *Nucl. Instrum. Meth.* **A499** (2003) 280-315.

[20] L. Rossi, "The LHC superconducting magnets" Particle Accelerator Conference 2003 141-145.

[21] A. D. McInturff, et al., "Test results for a high field (13 T) Nb3Sn dipole", Particle Accelerator Conference 1997 3212-4.

[22] G. L. Sabbi, et al., "Design of HD2: a 15T Nb_3Sn dipole magnet with a 35 mm bore", *IEEE Trans. Appl. Supercond.* **15** (2005) 1128-31.

[23] P. Ferracin, et al., "Development of the EuCARD Nb3Sn dipole magnet FRESCAII, IEEE Trans. Appl. Supercond., vol. 23, no. 3, Jun. 2013, Art. ID. 4002005.

[24] B. Caiffi, et al., "16 T cos θ dipoles for the Future Circular Collider", these proceedings.

[25] A. Asner, et al., "First Nb_3Sn, 1m long superconducting dipole model magnets for LHC break the 10 Tesla threshold", proceedings of MT-11 (Elsevier Applied Science, London and New York, 1989) 36-41, also LHC Note 105 (1989).

[26] H. J. Ten Kate, et al, "Development of an experimental 10 T Nb_3Sn dipole magnet for the CERN LHC", *IEEE Trans. Magn.* **27** (1991) 1996-9.

[27] G. Ambrosio, et al., "Test results and Analysis of LQS03 third long Nb3Sn quadrupole by LARP," IEEE Trans. Appl. Supercond., vol. 23, 2013, Art. ID. 4002204.

[28] L. Cooley, et al., "Industrial production of Nb_3Sn conductors for particle accelerator magnets", these proceedings.

[29] B. Bordini, et al., "The bundle barrier PIT wire developed for the HiLUmi LHC project," IEEE Trans. Appl. Supercond., vol. 27, 2017, Art. ID. 6000706.

[30] J. Fleiter, et al., "Optimization of the Nb_3Sn Rutherford Cable Geometry for the High-Luminosity LHC," IEEE Trans. Appl. Supercond., vol. 27, 2017, Art. ID. 4004305.

[31] J. Fleiter, et al., "Characterization of Nb3Sn Rutherford cable degradation due to strand cross-over", these proceedings.

[32] J. Troitino, "Applied metrology in the production of superconducting model magnets for particle accelerators", IEEE Trans. Appl. Supercond. Vol. 28 (2018), in press.

[33] A. Tollestrup, "Care and training in superconducting magnets" IEEE Trans Magn. Vol. 17, 1981 863-72.

[34] B. Bordini et al., "Critical Current Measurements of high-J_c Nb_3Sn Rutherford Cables Under Transverse Compression", IEEE Trans. Appl. Supercond., vol. 24, 2014, Art. ID. 9501005.

[35] E. Todesco, "Quench limits in the next generation of magnets", CERN Yellow Report 2013-006.

[36] S. Izquierdo Bermudez, et al., "Overview of the Quench Heater Performance for MQXF, the Nb_3Sn low-beta Quadrupole for the High Luminosity LHC", these proceedings.

[37] E. Ravaioli *et al*., "Advanced Quench Protection for the Nb3Sn Quadrupoles for the High Luminosity LHC," IEEE Trans. Appl. Supercond., vol. 26, 2016, Art. ID. 4002006.